

THE REDSHIFT DISTRIBUTION OF GIANT ARCS IN THE SLOAN GIANT ARCS SURVEY

MATTHEW B. BAYLISS^{1,2}, MICHAEL D. GLADDERS^{1,2}, MASAMUNE OGURI³, JOSEPH F. HENNAWI⁴, KEREN SHARON²,
BENJAMIN P. KOESTER^{1,2}, HÅKON DAHLE⁵*Draft version November 21, 2019*

ABSTRACT

We measure the redshift distribution of a sample of 28 giant arcs discovered as a part of the Sloan Giant Arcs Survey (SGAS). Gemini/GMOS-North spectroscopy provides precise redshifts for 24 arcs, and “redshift desert” constraints for the remaining 4. This is a direct measurement of the redshift distribution of a uniformly selected sample of bright giant arcs, which is an observable that can be used to inform efforts to predict giant arc statistics. Our primary giant arc sample has a median redshift $z = 1.821$ and nearly two thirds of the arcs – 64% – are sources at $z \gtrsim 1.4$, indicating that the population of background sources that are strongly lensed into bright giant arcs resides primarily at high redshift. We also analyze the distribution of redshifts for 19 secondary strongly lensed background sources that are not visually apparent in SDSS imaging, but were identified in deeper follow-up imaging of the lensing cluster fields. Our redshift sample for the secondary sources is not spectroscopically complete, but combining it with our primary giant arc sample suggests that a large fraction of *all* background galaxies which are strongly lensed by foreground clusters reside at $z \gtrsim 1.4$. Kolmogorov-Smirnov (KS) tests indicate that our well-selected, spectroscopically complete primary giant arc redshift sample can be reproduced with a model distribution that is constructed from a combination of results from studies of strong lensing clusters in numerical simulations, and observational constraints on the galaxy luminosity function.

Subject headings: gravitational lensing: strong — galaxies: clusters: general — galaxies: high-redshift

1. INTRODUCTION

Comparisons of the observed giant arcs counts against theoretical predictions provide a test for cosmological models of structure formation. Giant arc statistics depend on the growth of structure through the abundance and internal properties of the most massive galaxy clusters that dominate the giant arc cross-section. Bartelmann et al. (1998) suggested that there was an apparent order-of-magnitude discrepancy between the observed counts of giant arcs on the sky, and what is predicted by a Λ CDM cosmology. Subsequent comparisons of homogeneous samples of giant arcs against theoretical predictions have provided additional evidence for an apparent “giant arc problem” (Gladders et al. 2003; Zaritsky & Gonzalez 2003), though the samples remain of order a handful in size and therefore subject to prohibitively large uncertainties due to small number statistics.

Further studies have explored a variety of factors that could explain the underabundance of giant arcs predicted by theoretical models. Factors such as accounting for galaxies by painting them onto simulated dark matter halos (Flores et al. 2000; Meneghetti et al. 2000; Puchwein & Hilbert 2009), steepening of the gravita-

tional potential in cluster cores due to baryonic dissipation effects (e.g., Puchwein et al. 2005; Rozo et al. 2008), contributions from secondary structures along the line of sight (Puchwein & Hilbert 2009), accounting for short time-scale increases in the lensing cross-sections of halos due to mergers (Torri et al. 2004), and varying the redshift distribution of the population of background sources available to be strongly lensed into giant arcs (Hamana & Futamase 1997; Oguri et al. 2003; Wambsganss et al. 2004). Hennawi et al. (2007) found this last factor – the background source distribution – to be the one of the leading sources of uncertainty in their efforts to produce precise estimates for giant arc statistics from ray-tracing of dark matter simulated halos for a given cosmology. The primary motivation for studying giant arc statistics in a cosmological context is to provide a comprehensive test for models of large scale structure, which requires *a priori* constraints other model inputs, such as the properties of the background source population. Fortunately, the redshift distribution of giant arcs is directly observable given a sufficiently large and well-selected sample of giant arcs with redshift measurements. Samples of giant arc redshifts exist in the literature, including the catalog compiled by Sand et al. (2005) and the redshifts used by Richard et al. (2009), but they cannot be used to study the true redshift distribution of arcs because of their non-uniform selection and severe spectroscopic incompleteness.

In this letter we measure the redshift distribution of a spectroscopically complete sample of 28 giant arcs that were discovered in the Sloan Giant Arc Survey (SGAS; M. D. Gladders et al., in preparation) and targeted for multi-object spectroscopy with Gemini/GMOS-North. Our sample of giant arc redshifts is supplemented with a secondary sample of 19 additional strongly lensed sources

mbayliss@oddjob.uchicago.edu

¹ Department of Astronomy & Astrophysics, University of Chicago, 5640 South Ellis Avenue, Chicago, IL 60637² Kavli Institute for Cosmological Physics, University of Chicago, 5640 South Ellis Avenue, Chicago, IL 60637³ Division of Theoretical Astronomy, National Astronomical Observatory of Japan, 2-21-1 Osawa, Mitaka, Tokyo 181-8588, Japan⁴ Max-Planck-Institut für Astronomie K’önigstuhl 17, D-69117, Heidelberg, Germany⁵ Institute of Theoretical Astrophysics, University of Oslo, P.O. Box 1029, Blindern, N-0315 Oslo, Norway

that do not meet the selection criteria for our primary giant arc sample. For comparison we test the redshift distributions of our primary and secondary samples against simple models for the redshift distribution of giant arcs.

All magnitudes given in this letter are AB, calibrated relative to the SDSS (York et al. 2000).

2. DATA AND SAMPLES

2.1. Giant Arc Redshift Sample

The lensed background sources discussed in this letter are located near the cores of foreground massive galaxy clusters with a median redshift, $z_l = 0.435$, and a median dynamical mass, $M_{Vir} = 5.36 \times 10^{14} M_\odot h_{0.7}^{-1}$ (Bayliss et al. 2010). We take published spectroscopic redshifts from Bayliss et al. (2010), and use optical colors combined with the absence of specific spectral features to identify upper and lower redshift bounds for some arcs that lack precise spectroscopic redshifts. Given the spectral coverage of the Gemini/GMOS spectroscopy presented in Bayliss et al. (2010) we expect to observe one or more prominent emission lines (e.g. O[II] $\lambda 3727\text{\AA}$, H- β $\lambda 4861\text{\AA}$, O[III] $\lambda 4959, 5007\text{\AA}$ and H- α $\lambda 6563\text{\AA}$) for blue star-forming galaxies at $z \lesssim 1.5$, with some slight variation in this redshift limit that depends on the exact spectral coverage for each source. For strongly lensed sources at $1.5 \lesssim z \lesssim 3.3$ we must rely on rest-frame UV features to measure redshifts, but the strength of these features can vary significantly depending on the physical properties of the individual galaxies, such as metallicity and star formation history. At redshifts of $z \gtrsim 3.3$ we expect to see a broadband flux decrement that would be indicative of the Lyman- α Forest and Lyman Limit being redshifted well into the g -band, as well as strong absorption or emission from Lyman- α $\lambda 1216\text{\AA}$ redshifted into the data for sources with spectral coverage extending sufficiently bluerward.

Using the criteria outlined above we identify six arcs in the Bayliss et al. (2010) Gemini/GMOS data for which we can confidently place lower and upper limits on the redshifts. These six arcs all have blue colors in the available photometry, and their optical spectra consist of blue continuum emission with no strong absorption or emission features. The precise redshift constraints vary slightly from arc to arc, depending on the exact limits of the wavelength coverage, and are given in Table 1.

2.2. Primary Giant Arc Sample

Our primary giant arc sample includes only arcs that meet two criteria: 1) they were visually identified in the original SDSS imaging data and 2) they were observed spectroscopically with Gemini/GMOS-North. Our primary giant arc span a range in integrated g -band magnitude of $20.69 \leq g \leq 22.81$, as shown in Figure 1. This sample includes all sources identified as primary giant arcs in Bayliss et al. (2010), plus four additional arcs with redshift desert constraints as described in Section 2.1 above (those designated as “Primary” in Table 1). We are spectroscopically complete for the entire primary sample.

2.3. Secondary Background Source Sample

Our sample of secondary background sources includes objects that appear to be strongly lensed but lack the

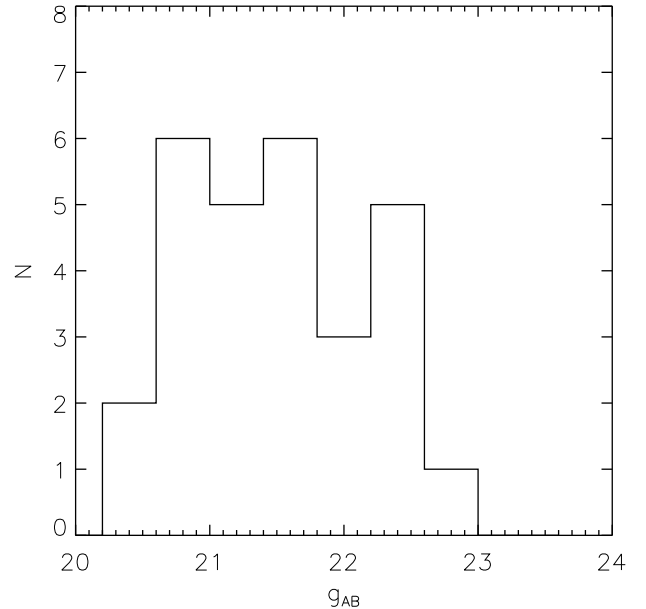


FIG. 1.— Histogram of g -band magnitudes for the 28 primary giant arcs discussed in this letter.

brightness and/or morphology to be identified in the visual selection processes that produced our primary giant arc sample. Most of these source were identified in the Gemini/GMOS pre-imaging data described in (Bayliss et al. 2010) and are designated as “secondary strongly lensed sources” in that paper. Secondary sources include one arc around each of SDSS J1115+5319 and GH0 132029+315500 that were identified in a search for giant arcs that is described in Hennawi et al. (2008). The most obvious giant arcs around each of SDSS J1115+5319 and GH0 132029+315500 have no precise redshift measurements, but their spectra exhibit featureless blue continuum emission that we use to derive upper and lower limits on the source redshifts. RCS2 J1055+5547 was discovered as a part of the RCS2 Giant Arc Survey, in which we apply a visual inspection similar to that used for the Sloan Giant Arc Survey, but using imaging data from the Second Red-Sequence Cluster Survey (RCS-2). RCS-2 imaging data is ~ 2 magnitudes deeper than the SDSS and has better median seeing ($\sim 0.7''$), resulting in a significantly different selection function from the SGAS. The secondary sample selection is not as uniform as the primary sample, and is spectroscopically incomplete, as there were numerous candidate secondary strongly lensed sources that were targeted in the Gemini observations of Bayliss et al. (2010) for which the data do not provide a redshift. We include the secondary sample in our analysis for the purpose of comparison against both our primary sample and our model arc redshift distributions.

3. THE REDSHIFT DISTRIBUTION OF GIANT ARCS

3.1. Models

Efforts to produce theoretical predictions for the abundance of giant arcs have modeled the population of back-

TABLE 1
REDSHIFT CONSTRAINTS FROM GEMINI SPECTROSCOPY

Cluster Core	Label ^a	z_{arc} range	l/w^b	R_{arc}^c	AB Mag ^d	Source Type
SDSS J1028+1324	C	$1.58 \leq z \leq 3.3$	14	$17''$	$g = 22.81$	Primary
SDSS J1115+5319 ^e	A	$1.45 \leq z \leq 3.2$	10	$31''$	$g = 23.03$	Secondary
SDSS J1152+0930	D	$1.56 \leq z \leq 3.3$	18	$14''$	$g = 22.54$	Primary
GHO 132029+315500 ^e	A	$1.5 \leq z \leq 3.3$	20	$21''$	$g = 22.59$	Secondary
SDSS J1446+3033	F	$1.45 \leq z \leq 3.3$	7	$15''$	$g = 22.42$	Primary
SDSS J1456+5702	B	$1.55 \leq z \leq 3.3$	7	$17''$	$g = 20.83$	Primary

^a Labels identify arcs in figures and tables that can be found in Bayliss et al. (2010)

^b Length-to-width ratios are all estimated from ground-based imaging with variable seeing, and generally represent lower limits on the true l/w for each arc. In the case of multiple arcs/images of a single source, the component with the largest length-to-width ratio is used.

^c The values reported here are measured by calculating the mean distance from a giant arc to the BCG of the lensing cluster, and serve as rough empirical estimates of the Einstein Radius for a given arc.

^d Reported values are integrated aperture magnitudes for the brightest contiguous piece of each arc.

^e These arcs were not identified in visual inspection of SDSS survey imaging, but rather in other imaging data of red sequence selected galaxy clusters.

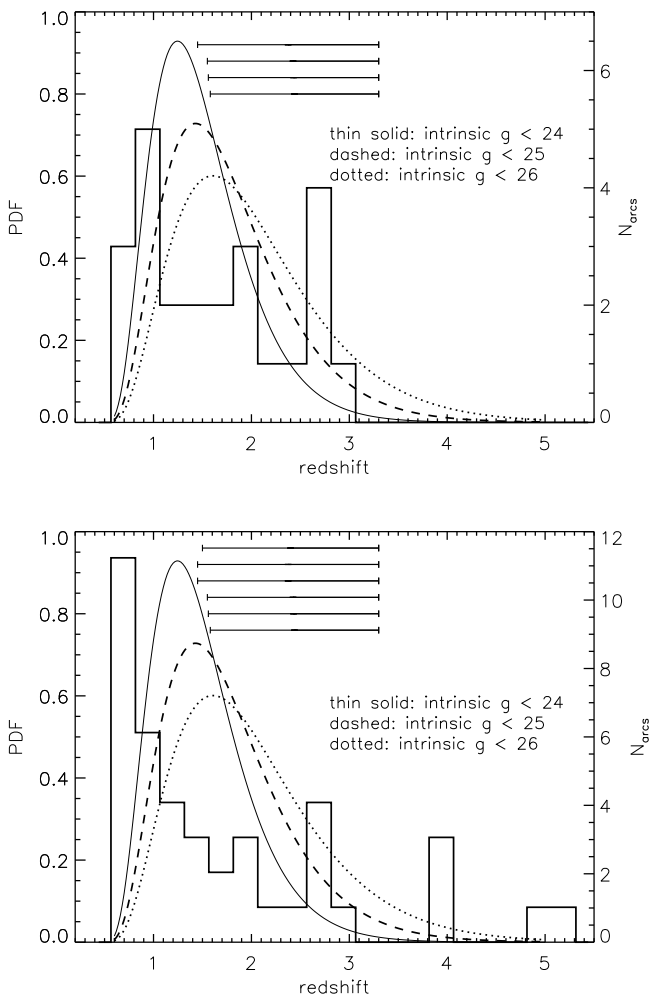


FIG. 2.— *Top* : The distribution of redshifts for the primary giant arc sample is plotted as the solid histogram with binsize $\Delta z = 0.25$. Arcs with redshift desert constraints are plotted as horizontal error bars indicating the upper and lower redshift limits for each arc. Over-plotted are three models for the expected redshift distribution, described in Section 3.1. *Bottom* : The same models as in the top panel, plotted with the redshift distribution for our giant arc plus secondary source combined sample. This combined sample redshift distribution is not compatible with any of the model redshift distributions.

ground sources galaxies in a variety of ways. It is known that the redshift distribution of background sources can have a dramatic impact on the giant arc statistics produced for a given cosmology (Hamana & Futamase 1997; Oguri et al. 2003; Wambsganss et al. 2004). Even more problematic is the fact that the uncertainty in the redshift distribution of background sources available to be lensed is effectively degenerate with the integrated lensing cross-section of the foreground halo population, and therefore with key cosmological parameters that strongly impact the properties of halos. This degeneracy arises because the Einstein radius, θ_E , of a lens at a fixed redshift increases as the distance to the source plane increases through its dependence on the angular diameter distance to the source.

The simplest background source model is one that places all background sources at a common redshift (e.g., Bartelmann et al. 1998; Meneghetti et al. 2010), for example $z_s = 1$ or $z_s = 2$, with some number density on the sky. Efforts by some groups (Wambsganss et al. 2004; Dalal et al. 2004; Hennawi et al. 2007; Puchwein & Hilbert 2009; Oguri & Blandford 2009) used a more advanced approach with background galaxies are placed at several discrete source planes, incorporating empirical measurement of the density of galaxies in different redshift bins in order to capture the evolution of galaxy counts. The galaxy counts are typically taken from deep pencil-beam surveys, and Hennawi et al. (2007) point out that cosmic variance in such survey fields can be as large as 50%, with measurements of the galaxy density on the sky in different surveys differing by more than a factor of 2 in the same redshift bin. This discretized source plane model is an improvement relative to the single source plane approach, but still falls short of being physically realistic. Horesh et al. (2005) simulated giant arc statistics using the same clusters in Bartelmann et al. (1998) and use a background source distribution that is constructed entirely from photometric redshifts in the Hubble Deep Field (HDF). This model is encouraging in its use of a smooth redshift distribution, but the HDF is only 5 arcmin² and suffers from the dramatic cosmic variance uncertainties Hennawi et al. (2007).

For the purpose of comparing against the giant arc redshift sample we construct a simple model which attempts to predict the redshift distribution of giant arcs

as function of the limit on the *intrinsic* brightness of background sources that are distorted into detectable giant arcs. This approach is equivalent to setting a limiting magnitude in the apparent brightness of giant arcs and assuming a uniform magnification by which all sources are boosted. In reality different sources will be magnified by varying amounts depending on the details of each lens-source interaction, so that there will not be a hard limiting magnitude in intrinsic source brightness. Assuming typical total magnifications of $\sim 10 - 25$, and noting an approximate integrated limiting magnitude of $g \lesssim 22.5$ for our primary giant arc sample, we produce model giant arc redshift distributions for two cases: 1) an intrinsic limiting source magnitude, $g_{lim} < 25$ and 2) $g_{lim} < 26$. For the purpose of comparison we also produce a model redshift distribution for an intrinsic limiting source magnitude of $g_{lim} < 24$, which has a peak in the probability distribution closer to $z_s = 1$.

Our model for the giant arc redshift distribution is calculated as follows: for the arc cross-section, σ_{arc} , we adopt the scaling relation derived by Fedeli et al. (2010), which is based on large volume N-body simulations. The Fedeli et al. (2010) cross-section is defined from simulated arcs with length-to-width ratio, $l/w \gtrsim 7.5$, all of which are produced from sources at a redshift, $z_s = 2$. We derive the arc cross-sections for different source redshifts assuming a universal matter density profile slope of -1.5 in the region around the Einstein radii for cluster lenses. The redshift distribution of source galaxies for a given magnitude limit, dn/dz_s , is estimated using the photometric redshift catalog in the 2 deg² COSMOS field (Ilbert et al. 2009). We then compute the expected redshift distribution of giant arcs by the equation:

$$\frac{dp_{arc}}{dz_s} = \frac{\sigma_{arc} \frac{dn}{dz_s}}{\int dz_s \sigma_{arc} \frac{dn}{dz_s}}$$

The length-to-width limit used to define the arc cross section scaling relation in Fedeli et al. (2010) is consistent with the length-to-width lower limits on our sample of giant arcs as measured from ground-based imaging data (Bayliss et al. 2010).

3.2. Properties of the SGAS Giant Arc Redshift Distribution

The redshift distribution for our primary giant arc sample is shown in Figure 2, along with models for giant arc redshift distributions that we derived in the previous section. Figure 2 also includes a plot of our primary giant arc redshift sample combined with our spectroscopically incomplete sample of secondary source redshifts. We use the KS test to quantify the agreement between our measured redshift distributions and the proposed models. Conducting KS tests on the data requires that we correctly account for the giant arcs in our sample with constraints that place them in the redshift desert. To do this we use the information that we have about the distribution of giant arcs within the redshift desert: the precise redshifts that we measure for 13 – 14 giant arcs that are located within the redshift desert (the number depends on the exact redshift desert constraints).

We produce many Monte Carlo realizations of the redshift distribution by assigning a precise redshift for each

redshift desert arc that is drawn randomly from our sample of giant arcs that *do* have precise redshifts within the corresponding upper and lower redshift bounds. This method assumes that our giant arcs with precise redshifts between $1.45 \lesssim z \lesssim 3.3$ are distributed within that range in the same way as our giant arcs that have only redshift desert constraints. This assumption is not necessarily valid, but we have no strong evidence to contradict it, so we consider it to be the most robust method of including the giant arcs with upper and lower redshift bounds in the statistic tests. Realizations that draw precise redshifts at random from within the upper and lower bounds for a given redshift desert arc produce distributions that are indistinguishable from the realizations that draw redshifts from our sample within those bounds, which indicates that giant arcs with precise redshifts that fall within the redshift desert, $1.5 \lesssim z \lesssim 3.3$, are indistinguishable from being evenly distributed within that range.

We also explore alternative ways of handling those arcs with redshift desert constraints in order to explore how the two extreme possible deviations from the Monte Carlo realization method described above affect the results of the KS tests. The first extreme corresponds to the case where all redshift desert arcs have true redshifts at or near their lower redshift bound, and the opposite extreme where all redshift desert arcs have true redshifts that are at or near their upper redshift bound. This gives us three different giant arc redshift samples that span the range of possible true redshift distributions for our complete primary giant arc sample.

The realizations for our primary giant arc sample are tested against our models to produce average KS probabilities of the likelihood that the redshift data are drawn from the model distributions. We perform another series of KS tests on the combined primary giant arc plus secondary source samples, where the two secondary arcs with redshift desert constraints are handled in exactly the same three ways as the redshift desert primary giant arcs. Results from all KS tests are shown in Table 2, and from these results we infer that the redshift distribution of our giant arc sample is moderately well described by the our simple arc redshift distribution model tuned to the range of intrinsic limiting magnitudes that correspond to a reasonable range of total magnifications, $\sim 10 - 25\times$. The best agreement between our giant arc redshift sample and the model redshift distributions occurs when the arcs with redshift desert constraints are assumed to have true redshifts at or near their lower redshift bound; in this case the data have a $\sim 74\%$ chance of being drawn from the same probability distribution as the model corresponding to a limiting intrinsic source magnitude of $g_{lim} < 25$. There is some reason to expect that our arcs with redshift desert constraints may be more likely to have true redshifts closer to the lower end of the allowable range because of the spectral features that fall into our observed wavelength range. For example, at $1.6 \lesssim z \lesssim 2.3$ we must rely on lines such as MgII $\lambda 2796, 2803\text{\AA}$, and FeII $\lambda 2344, 2372, 2384, 2586, 2600\text{\AA}$, which tend to be relatively weak compared to bluer features, such as CIV $\lambda 1448, 1551\text{\AA}$, SiII $\lambda 1260, 1527\text{\AA}$, and SiIV $\lambda 1394, 1403\text{\AA}$.

It is also interesting to note that a redshift sample

TABLE 2
KOLMOGOROV-SMIRNOV TESTS OF REDSHIFT DISTRIBUTIONS

Redshift Sample	Redshift Desert ^a	Probability for $g_{lim} < 24$	Probability for $g_{lim} < 25$	Probability for $g_{lim} < 26$
Primary	monte carlo	0.0029	0.1647	0.2507
Primary	minimum	0.0613	0.7381	0.1279
Primary	maximum	0.0003	0.0502	0.2508
Primary + Secondary	monte carlo	0.0014	0.0132	0.0021
Primary + Secondary	minimum	0.0329	0.0132	0.0007
Primary + Secondary	maximum	4.050e-05	0.0019	0.0021

^a This column indicates how arcs with redshift desert constraints were handled in the tests. “Monte Carlo” indicates the same where redshift desert arcs are given precise redshifts drawn randomly from the sample of giant arc redshifts that lay within their respective upper and lower redshift bounds, “minimum” indicates that all redshift desert sources were set to have redshifts equal to the lower bound on their possible redshift range, and “maximum” indicates that all redshift desert sources were set to have redshifts equal to the upper bound on their possible redshift range.

which combines the primary giant arcs and the secondary strongly lensed sources is never in good agreement with our model redshift distributions, which underscores the importance of using well-selected and spectroscopically complete redshift samples to study giant arc redshift distributions.

It is possible that our giant arc redshift distribution could be biased high relative to the true redshift distribution of SGAS giant arcs due to a systematic selection effect. Targets were selected for Gemini spectroscopy with a preference toward systems with larger apparent arc radii, R_{arc} , which is measured as the average angular separation between an arc and the center of the cluster lens – typically coincident with the brightest cluster galaxy. A selection based on large R_{arc} could bias our giant arcs toward having higher redshifts than if we had selected targets completely at random. However, our spectroscopic target selection was not based purely on R_{arc} , and as discussed in Bayliss et al. (2010) we expect that it does not have a strong impact on our results.

4. SUMMARY AND CONCLUSIONS

From the comparison of our redshift data against models for possible background source distributions we conclude that the data are consistent with a model that combines strong lensing cross-sections derived from simulations, galaxy counts from COSMOS, and the approximate brightness limit of our giant arc sample. Depending on how we treat our arcs with redshift desert constraints,

the model has a KS probability as high as 73% of having the same redshift distribution as our sample. Our primary giant arcs have a median redshift of $z = 1.821$, and approximately 64% (18/28) of the primary giant arcs are located at $z \gtrsim 1.45$, indicating that the background galaxies which are strongly lensed into bright giant arcs tend to reside at high redshift. This result is encouraging for future prospects to discover very large samples of bright, strongly lensed galaxies at high redshift that can be targeted for detailed individual study.

The analysis presented here represents an important step forward in studying the number and distribution of giant arcs produced by massive galaxy cluster strong lenses. While our current sample of giant arc redshifts is large compared to previous studies of strong lensing around clusters of galaxies, the numbers are still small enough to be subject to significant random fluctuations. Our catalog of redshifts for primary giant arcs is not so large that we can ignore Poisson errors, but our ability to precisely constrain the redshift distribution of arcs discovered in the SGAS will improve as we collect spectroscopy for a larger fraction of our full SGAS giant arc sample.

JFH acknowledges support provided by the Alexander von Humboldt Foundation in the framework of the Sofja Kovalevskaja Award endowed by the German Federal Ministry of Education and Research.

REFERENCES

- Bartelmann, M., Huss, A., Colberg, J. M., Jenkins, A., Pearce, F. R. 1998, *A&A*, 330, 1
 Bayliss, M. B., Hennawi, J. F., Gladders, M. D., Koester, B. P., Sharon, K., Dahle, H., Oguri, M., 2010, *ArXiv e-prints*, astro-ph/1010.2714
 Dalal, N. and Holder, G. and Hennawi, J. F. 2004, *ApJ*, 609, 50
 Fedeli, C., Meneghetti, M., Gottloeber, S., Yepes, G. 2010, *A&A*, 519, 91
 Flores, R. A., Maller, A. H., Primack, J. R. 2000, *ApJ*, 535, 555
 Gladders, M. D., Hoekstra, H., Yee, H. K. C., Hall, P. B., Barrientos, L. F. 2003, *ApJ*, 593, 48
 Hamana, T., Futamase, T. 1997, *MNRAS*, 287L, 7
 Hennawi, J. F., Dalal, N., Bode, P., Ostriker, J. 2007, *ApJ*, 654, 714
 Hennawi, J. F. et al. 2008, *AJ*, 135, 664
 Horesh, A., Ofek, E. O., Maoz, D., Bartelmann, M., Meneghetti, M., Rix, H.-W. 2005, *ApJ*, 633, 768
 Ilbert, O. et al. 2009, *ApJ*, 690, 1236
 Meneghetti, M., Bolzonella, M., Bartelmann, M., Moscardini, L., Tormen, G. 2000
 Meneghetti, M., Fedeli, C., Pace, F., Gottloeber, S., Yepes, G., 2010, *A&A*, 519, 91
 Oguri, M. & Blandford, R. D. 2009, *MNRAS*, 392, 930
 Oguri, M., Lee, J., Suto, Y. 2003, *ApJ*, 599, 7
 Puchwein, E. and Bartelmann, M. and Dolag, K. and Meneghetti, M. 2005, *A&A*, 442, 405
 Puchwein, E. & Hilbert, S. 2009, *MNRAS*, 398, 1298
 Richard, J. et al. 2010, *MNRAS*, 404, 325
 Rozo, E., Nagai, D., Keeton, C., Kravtsov, A. 2008, *ApJ*, 687, 22
 Sand, D. J., Treu, T., Ellis, R. S., Smith, G. P. 2005, *ApJ*, 627, 32
 Torri, E., Meneghetti, M., Bartelmann, M., Moscardini, L., Rasia, E. and Tormen, G. 2004, *MNRAS*, 349, 476
 Wambsganss, J., Bode, P., Ostriker, J. 2004, *ApJ*, 606, 93
 York, Donald G. et al 2000, *AJ*, 120, 1579
 Zaritsky, D. & Gonzalez, A. H. 2003, *ApJ*, 584, 691